DOI: 10.18462/iir.gl2022.48

Validation of a Modelica numerical model for pillow plate heat exchangers using phase change material

Sven FÖRSTERLING[(a)], Håkon SELVNES[(b)], Alexis SEVAULT[(b)]

[(a)] TLK-Thermo GmbH, 38106 Braunschweig, Germany
s.foersterling@tlk-thermo.com
[(b)] SINTEF Energy Research, Postboks 4761 Torgarden, 7465 Trondheim, Norway
hakon.selvnes@sintef.no, alexis.sevault@sintef.no

ABSTRACT

Refrigeration systems are often installed in industrial facilities where the difference between the peak and average thermal loads can be considerable due to the throughput of products and changes in the ambient conditions throughout the year. Cold Thermal Energy Storage (CTES) technologies can be introduced to increase the flexibility of such installations by decoupling the supply and demand of refrigeration. CTES systems based on the latent heat storage principle using Phase Change Materials (PCM) are preferred over sensible heat storage due to higher compactness, operation over a narrow temperature range and ability to tailor the storage temperature to each specific application.

The current study presents a numerical model of a CTES unit using PCM as the storage medium and CO_2 as refrigerant. The heat exchanger in the CTES unit consists of a stack of pillow plates immersed into a stainless-steel container filled with PCM. The charging and discharging processes of the PCM-CTES unit are carried out through evaporation and condensation of the CO_2 circulating inside the plates, respectively. The dynamic model of the PCM-CTES unit is developed in the object-oriented programming language Modelica using the component library TIL-Suite. The model of the PCM-CTES unit is validated by using previously published experimental data from a test facility with an identical setup. Various heat exchanger configurations, storage medium and refrigerant parameters are tested, and the model demonstrates good agreement with the experimental data.

Keywords: Thermal energy storage, Phase Change Material, Refrigeration, CO2 refrigeration, Dynamic model, Modelica, Pillow plate heat exchanger

1. INTRODUCTION

More renewable energy means a more variable power grid, accelerating the need to develop more energy-efficient industry. Better energy storage solutions can reduce peak power demand for intermittent processes, ease load shifting, and safeguard against power supply bottlenecks. Compared to traditional electricity storage, Thermal Energy Storage (TES) stores large amounts of thermal energy at both low- and high temperatures more efficiently and at much lower cost. Although very relevant for food industry, Cold TES (CTES) know-how is still limited.

To meet this challenge, the PCM-STORE project is developing low-temperature TES systems based on Phase Change Materials (PCM) for industrial cooling and freezing processes (Sevault, 2020). Three case studies representing different temperature ranges are identified as potential candidates for implementation of PCM-CTES: industrial batch freezing processes, cold storage in food processes, and refrigerated display cabinet cases (Jokiel et al., 2021; Selvnes et al., 2019, 2021a; Sevault et al., 2018; Hafner and Nekså, 2018; Manescu et al., 2017; Fidorra et al., 2015, 2016).

Leveraging PCM-CTES will enable industry to cover their peak cooling needs while reducing peak power demand, increasing cooling capacity and reducing food waste. This will reduce both operational and investment costs and lead to a more sustainable industry (Fidorra et al., 2021). An additional advantage of

This is the accepted version of a paper published at GL2022
http://dx.doi.org/10.18462/iir.gl2022.0048

CTES for food industry, technology suppliers and grid operators is to use CTES as thermal battery combined intermittent renewables energy (solar PV, etc). However, this solution currently not explored to a great extent in the literature.

The main objective of PCM-Store is to develop the knowledge required to implement affordable and efficient low-temperature PCM thermal energy storage units (PCM-CTES) for food industry. One goal is the development of new PCM-Store heat exchanger concepts such as pillow-plate geometry-based storages, which are considered numerically in this publication. The literature includes publications on experimental studies of pillow plates integrated in PCM-CTES heat exchangers (Selvnes, 2021b) and detailed CFD modelling of ice formation and melting processes (Selvnes, 2019a, 2019b) and fluid flow through the plates without PCM material (Mitrovic and Maletic, 2011; Piper et al., 2015a, 2015b; Tran et al., 2018). Bony and Citherlet (2007) present a TRNSYS model for PCM storage in a solar system and Mehling (2008) mentions a Modelica model for the design of phase change slurry systems. Neumann (2020) presents models for high temperature PCM storage systems with plates.

In this publication, a numerical dynamic model with Modelica for simulating a PCM storage using a pillow plate heat exchanger geometry for cold storage is presented. The model is validated with dynamic measurement data from Selvnes (2021b) using water as PCM, which freezes and melts at a temperature of 0 °C, and CO_2 as the refrigerant. The model was developed for both component design and system simulation and can be used to optimize and study the heat exchangers and systems in the PCM-Store project (Figure 1). Important goals and boundary conditions for model development include investigation and design options for the PCM storage geometry, system design with additional cooling or refrigeration circuit components, dynamic switching processes, real-time simulation for controller design and annual simulation, evaluation tools for various cooling fluids and refrigerants and PCM materials. The model allows flexible use with different PCMs in different temperature ranges and thus enables a wide range of possible uses in future applications.

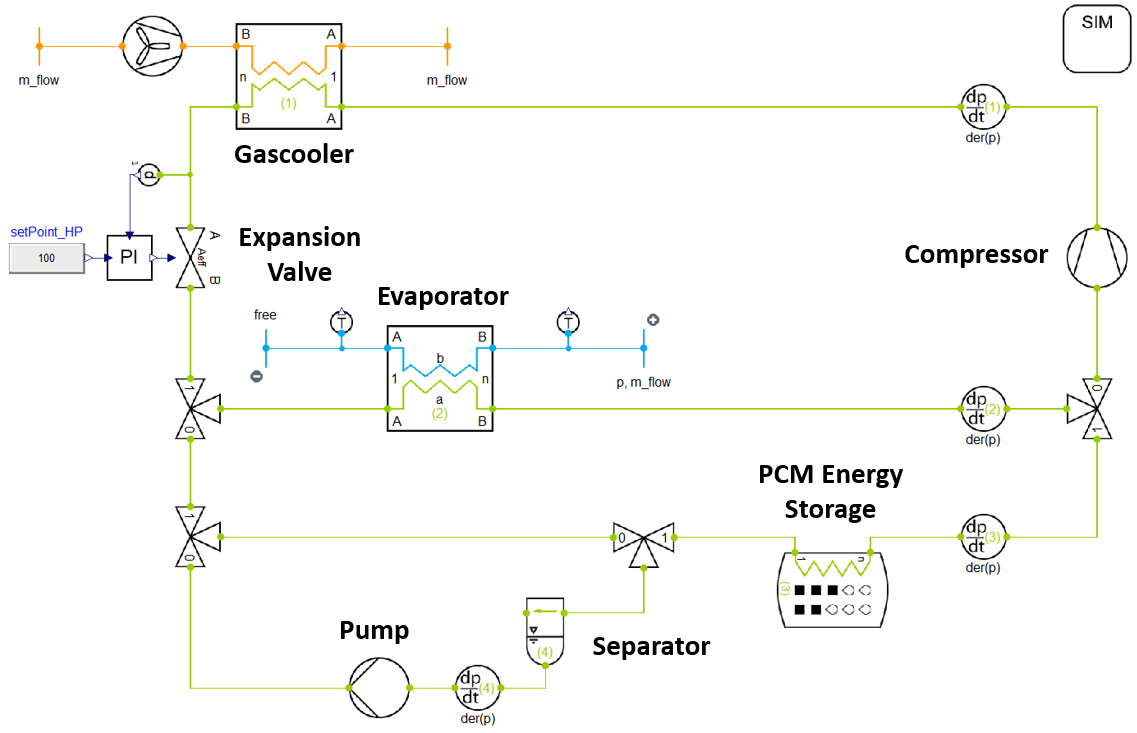

Figure 1: Simulation model layout for an industrial refrigeration system with PCM energy storage with TIL-Suite (Tegethoff, 2011). Various directional control valves enable flexible switching processes from cooling operation into parallel charging and discharging with a refrigeration pump.

This is the accepted version of a paper published at GL2022
http://dx.doi.org/10.18462/iir.gl2022.0048

2. SIMULATION MODEL

A simulation model was developed to investigate the stationary and dynamic behaviour of thermal energy storages with PCM. The model can be used for system simulation and component design and development. Other important areas of application are real-time simulations e.g., for annual simulations, controller design, e.g. for predictive control applications and hardware in the loop capability.

The model was programmed in the object-orientated language Modelica (Modelica Association, 2022) and implemented within the simulation environment Dymola and is available in the AddOn library PCM Storages of the TIL-Suite library. TIL-Suite is a Modelica model library for thermal components and systems (Tegethoff, 2011 and Richter, 2008) using TILMedia-Suite as software package for calculating the properties of thermophysical substances (Schulze, 2013).

The TIL AddOn library PCM Storages shown in Figure 2 is intended for simulation of thermal storage systems with a variety of heat exchanger geometries, such as fin-and-tube, tube, plate, pillow-plate and other geometry types. Other geometry types can be added using the basic model structures. Based on the property library TILMedia different fluid types like liquids, refrigerants and gases and combinations can be selected for the flow through the tubes and channels. Various PCMs can be used as a storage medium or implemented by the user.

With the supplied substance library with PCM or so called SLE-Medium (solid-liquid equilibrium medium), system simulation can be carried out with different storage media at different temperature levels. Energy can be stored or released, e.g. phase change processes through freezing, melting and possibly crystallization of metastable states of supercooled liquids. Further user-specific PCM data can be implemented via the TILMedia interface.

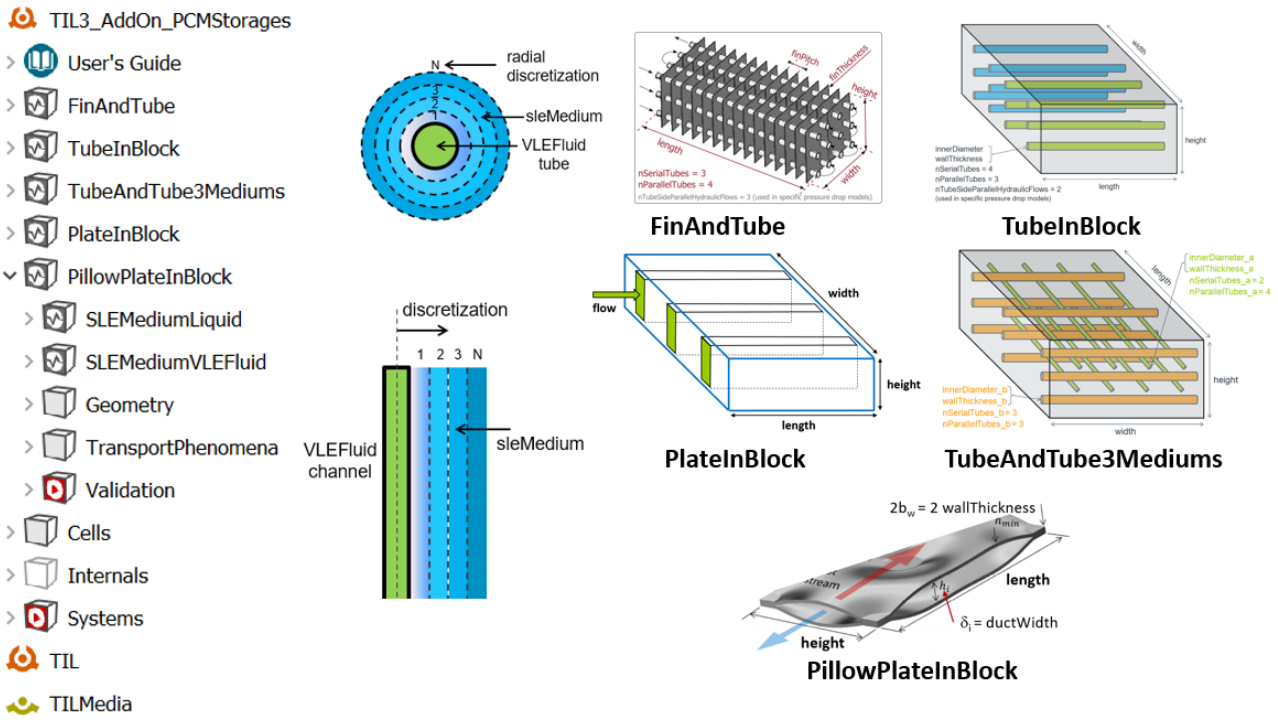

Figure 2: TIL AddOn PCM Storages library package structure with different heat exchanger geometries, flow channel arrangement using tubes and plates through which different types of fluid types such as liquid, refrigerant and air flow through them and are in thermal contact with the PCM material in between.

This is the accepted version of a paper published at GL2022
http://dx.doi.org/10.18462/iir.gl2022.0048

2.1. Model structure and main equations

The available storage devices are sorted by their geometry type and then by the media types flowing through them. Almost all thermal heat storage models of this library use a similar model structure including a finite volume-based approach. Figure 3 shows the Model structure of the pillow-plate heat exchanger model with SLE-storage, showing the VLE (vapour-liquid equilibrium) cell discretization in refrigerant flow direction and perpendicular to the flow direction in the SLE material direction.

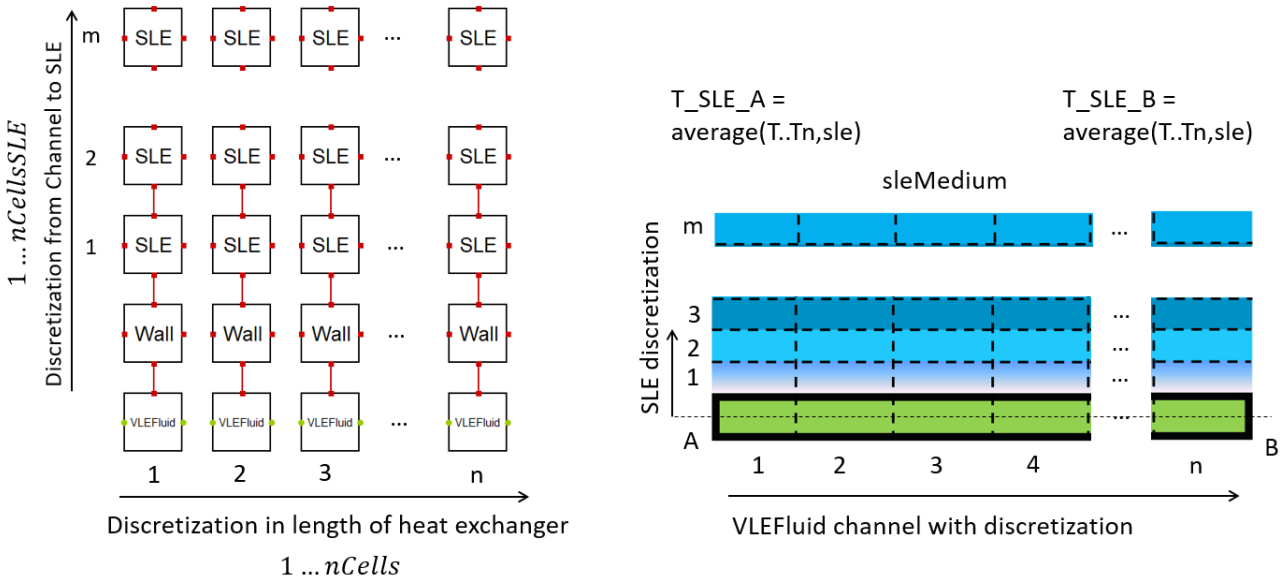

Figure 3: Model structure of the pillow-plate heat exchanger with SLE-storage showing the VLE cell discretization in refrigerant flow direction and perpendicular in SLE material direction.

The main model structure is a series connection of following cells: VLE-Fluid, Liquid or Gas cells in the flow channel, each connected to Wall cells and SLE-Fluid cells. The storage system is discretized in two directions: first, along the length of the flow channel, and second perpendicular to the flow direction in the direction from the flow channel to the SLE material.

As shown in Figure 4, the SLE-Cell consists of 4 heat ports in four possible heat transfer directions to north, south, west and east. The SLE medium model object from TILMedia calculates the thermophysical property data with given inputs: pressure (p), enthalpy (h) and the parameter sleMediumType. In this study, heat transfer between wall and SLE cells is considered only perpendicular to the refrigerant flow direction in north-south-direction, assuming that heat transfer between the cells in east-west direction parallel to the refrigerant flow is negligible compared to heat transfer in north-south direction.

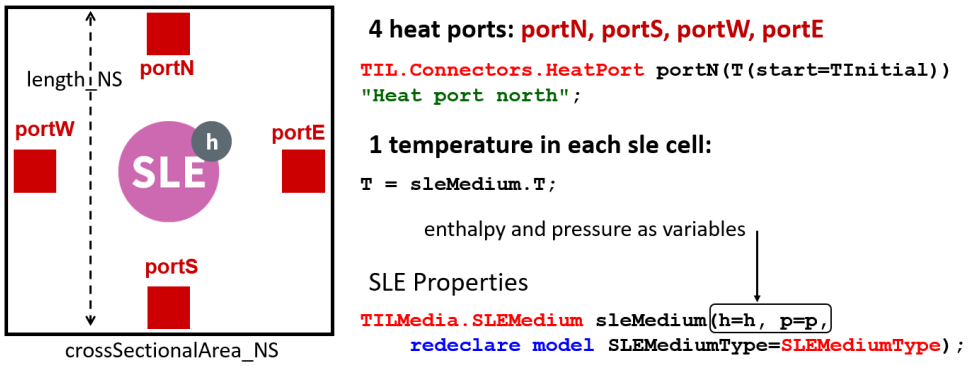

Figure 4: Structure of TIL SLE-Cell.

This is the accepted version of a paper published at GL2022
http://dx.doi.org/10.18462/iir.gl2022.0048

The SLE mass calculation is carried out using the initial values for temperature at time zero and stays constant while the volume varies due to variable SLE density:

$$m_{sle} = V_{sle,ini} \cdot \rho_{sle,ini} = V \cdot \varrho_{sle} \quad \text{and} \quad m_{sle} = V \cdot \rho_{sle} \,. \qquad \text{Eq. (1)}$$

The heat transfer $\dot{Q}_{sle,port}$ via the ports is defined by the following transport equation with the thermal conductivity λ_{sle}, the cell cross section area $A_{crossSection}$, the cell length, the temperature difference between the cell temperature and the heat port temperature and the number of plates n_{Plates}:

$$\dot{Q}_{sle,port} = \lambda_{sle} \cdot A_{crossSection} \cdot \frac{2}{length} \cdot (port.T - T) \cdot n_{Plates} \,. \qquad \textit{Eq. (2)}$$

For numerical reasons, the energy balance is formulated with the enthalpy as differential variable and the enthalpy can be calculated with TILMedia in dependency to the temperature:

$$m_{sle} \cdot \frac{dh_{sle}}{dt} = \sum \dot{Q}_{sle,port} \text{ with} \quad h_{sle} = h(T) \,. \qquad \textit{Eq. (3)}$$

SLEMedium can be solid, liquid or have a solid-liquid equilibrium (SLE). The SLE cell quality q, which describes the ratio of solid and liquid SLE material, is calculated as a function of following parameters $q = quality\_h\left(h, c_{p,solid}, c_{p,liquid}, h_{fusion}, T_{solid}, T_{liquid}\right)$. Using the SLE quality properties for heat capacity, density and thermal conductivity are calculated with a linear approach in the following way:

$$c_p = c_{p,solid} + \left(c_{p,liquid} - c_{p,solid}\right) \cdot q \qquad \textit{Eq. (4)}$$

$$1/\rho_{sle} = 1/\rho_{sle,solid} + \left(1/\rho_{sle,liquid} - 1/\rho_{sle,solid}\right) \cdot q \qquad \textit{Eq. (5)}$$

$$\lambda = \lambda_{solid} + \left(\lambda_{liquid} - \lambda_{solid}\right) \cdot q \qquad \textit{Eq. (6)}$$

Medium types for VLE-Fluid, Gas and Liquid can be defined in the SIM-Object. Properties for the SLE-Medium can be defined within the PCM-Storage model. The property data of water used within this project come from VDI Wärmeatlas (2012).

2.2. Geometry

The PillowPlateInBlock PCM-Storage arrangement shown in Figure 5 can be characterized as follows in terms of geometry: it is a rectangular block with internal pillow plates that form fluid channels for the flow of liquid fluid or refrigerant (VLE-Fluid), represented by green colour in Figure 5. The volume gaps between the pillow plate volumes and the rectangular storage block are filled with the PCM material (SLEMedium).

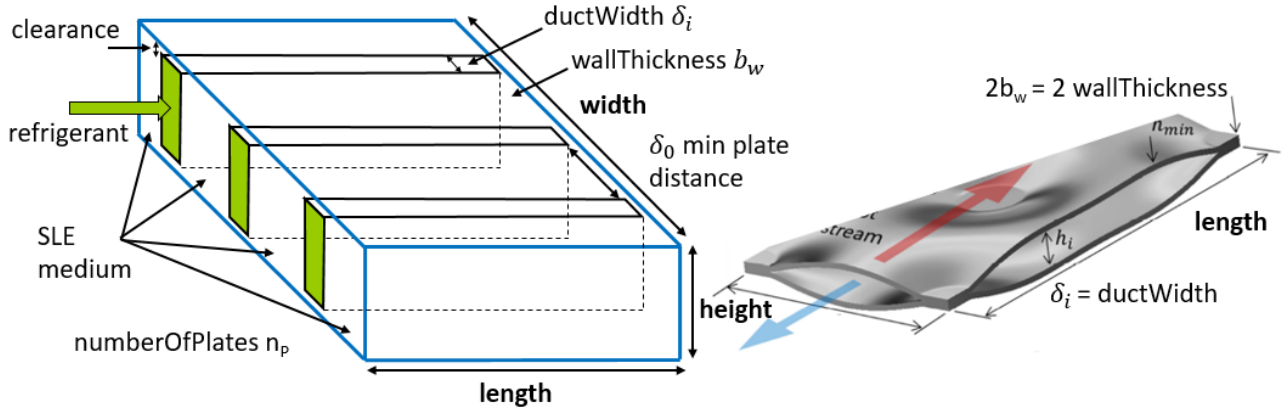

Figure 5: Geometry of pillow-plate SLE heat exchanger (Piper et al., 2015b).

This is the accepted version of a paper published at GL2022
http://dx.doi.org/10.18462/iir.gl2022.0048

The definition of the most important following pillow-plate specific design parameters and their approximations can be found e.g. in Piper et al. (2014, 2015b) and are used within the model as follows:

The increase in heat transfer from the pillow plate enlargement is about as large as the area from the welds. The following assumption with the active height and length of the plate in contact with the PCM material and the plate number is used for the ***heat transfer area***

$$A_{HT} \approx 2 \cdot \text{height} \cdot \text{length} \cdot n_p \,, \qquad \text{Eq. (7)}$$

using the plate length and the heat exchanger **width**

$$width = n_p \cdot (2b_w + \delta_0) \qquad \text{Eq. (8)}$$

which is calculated from the plate wall thickness b_w and the minimum plate distance δ_0.

The ***hydraulic diameter*** for the fluid flow channel

$$d_{hyd} = 2 \cdot \frac{\delta_i}{\sqrt{2}} \qquad \text{Eq. (9)}$$

is calculated with the maximum inner duct width

$$\delta_i = \delta_{outer,max} - 2b_w \qquad \text{Eq. (10)}$$

which is calculated with the maximum outer expansion width $\delta_{outer,max}$ and the plate wall thickness b_w.

The mean outer cross-sectional area of each plate

$$A_{outer,cross} = \delta_{mean,outer} \cdot height \qquad \text{Eq. (11)}$$

is calculated with the mean outer plate thickness

$$\delta_{mean,outer} = \frac{\delta_{min} + \delta_{max}}{2} \qquad \text{Eq. (12)}$$

the arithmetic mean value of outer minimum plate thickness $\delta_{min} = 2 \cdot \delta_w$ and the maximum plate thickness $\delta_{max} = 2 \cdot \delta_w + \delta_i$.

The internal hydraulic cross-sectional area

$$A_{hydraulic,inner} = \frac{\delta_i}{\sqrt{2}} \frac{height}{n_{serialHydraulicFlow}} \qquad \text{Eq. (13)}$$

is calculated with the hydraulic diameter Eq. (9), the plate height and the number of plate-side serial hydraulic flows

$$n_{serialHydraulicFlow} \cdot$$

The outer hydraulic cross-sectional area

$$A_{hydraulic,outer} = \delta_{mean,outer} \cdot \ height \qquad \text{Eq. (14)}$$

is calculated with the mean outer plate thickness Eq. (12) and plate height.

2.3. Heat transfer and pressure drop

The object-oriented model structure of the TIL library supports the interchangeability of the correlations that describe transport phenomena such as heat transfer and pressure drop (Tegethoff, 2011). Using the

This is the accepted version of a paper published at GL2022
http://dx.doi.org/10.18462/iir.gl2022.0048

definitions for the heat transfer area in Eq. (7), the hydraulic diameter in Eq. (9), and the inner hydraulic-cross sectional area in Eq. (13), the heat transfer and pressure drop in the pillow plate channels are calculated using the following correlations: The pressure drop in the two-phase flow is approximately calculated using Swamee-Jain correlation (Swamee and Jain, 1976). The following heat transfer correlations are applied for the fluid inside the pillow plate channel, depending on the process and flow regime:

For evaporation Shah Chen (Collier and Thome, 1996) is applied, for condensation the correlation of Shah (Shah, 1979) is applied, and for single-phase flow of superheated gas, subcooled and supercritical conditions the correlation of Gnielinski Dittus Boelter (Baehr and Stephan, 1996) were used.

3. VALIDATION

The model validation was carried out with measurment data from Selvnes et al. (2021b) for a pillow plate heat exchanger cold storage with water as the PCM between the plates. As refrigerant CO_2 was used as the circulating medium for charging and discharging the storage tank. Within the test facility, the pillow plates are stacked horizontally on top of each other with defined distance spacers in a container filled with water. Gravity convection of the water can therefore be neglected. Due to short operation times heat losses to the ambient are neglected. The geometry data of the investigated pillow plate heat exchanger are shown in Table 1. The length and height were kept constant, while the distance between the pillow plates and thus the space for the PCM was varied between 15, 30 and 45 mm.

On the refrigerant side, each plate is divided into 3 serial hydraulic flows with flow deflectors and all plates are flown through in parallel. On the outer perimeter of the plate there is an area where the plates are welded together with no refrigerant channel in between. This area does not primarily participate in heat transfer and is accounted for by an correspondingly reduced length, height and heat transfer area as shown in Fig. 1 in Selvnes et al. (2021b).

The mass of water and the initial volume are calculated using Eq. (1) with the initial density of the liquid (charging) or frozen water (discharging). Due to the difference in density between liquid and solid water at 0 °C of

$$\frac{\rho_{ice}}{\rho_{liquid}} = \frac{916.76\ kg/m^3}{999.84\ kg/m^3} = 0.917\ , \qquad \text{Eq. (15)}$$

there is a corresponding difference of mass and energy for charging and discharging.

The maximum charge and discharge latent energy is calculated as a reference using the water mass and the enthalpy of fusion:

$$E_{pcm,max,latent} = m_{water} \cdot \Delta h_{fusion} \text{ with } \Delta h_{fusion,water,0°C} = 332.5\ kJ/kg\ . \qquad \text{Eq. (16)}$$

Water mass and latent energy values are shown in Table 1 for the different plate distance arrangements.

A total of 12 validation measurement series were used, 6 for charging and 6 for discharging and two different refrigerant mass flows for each plate spacing (Selvnes et al., 2021b). Table 2 summarizes the important boundary conditions for the validation points: plate geometry, measurement time, measured refrigerant mass flow rate, inlet pressure and mean water initialization temperature. As shown in Figure 8, a total of 27 temperature sensors, distributed on three plates (2, 6, 9), placed at a distance of 2-3 mm from the plate surface and almost equally long sections along the internal serial flow channels in the water/ice layer record the dynamic temperature distribution within the PCM. The pressure difference on the refrigerant side is recorded by two pressure sensors at the inlet and outlet of the heat exchanger.

This is the accepted version of a paper published at GL2022
http://dx.doi.org/10.18462/iir.gl2022.0048

Table 1: Geometry and property data of the tested pillow-plate heat exchangers. The material data for water are taken from VDI Wärmeatlas (2012).

plate distance δ_0	[mm]	15	30	45
width*	[mm]	170	320	470
length (active)	[mm]	1480 (1455)	1480 (1455)	1480 (1455)
height (active)	[mm]	740 (680)	740 (680)	740 (680)
$n_{SerialHydraulicFlow}$	[-]	3	3	3
$A_{Heat\ Transfer}$ (active)	[m²]	21.9 (19.8)	3	3
V_{water}	[dm³]	127.1 dm³	275.5 dm³	424 dm³
$m_{water,charging}$ (ρ_{liquid} = 999.84 kg/m³)	[kg]	127.1	275.49	423.9
$m_{water,discharging}$ (ρ_{ice}= 916.76 kg/m³)	[kg]	116.6	252.6	388.7
$m_{wall,steel}$	[kg]	115	115	115
$Energy_{pcm,max,charging}$**	[kWh]	11.7	25.44	39.15
$Energy_{pcm,max,discharging}$	[kWh]	10.8	23.3	35.9

*width $= n_p(2 \cdot b_w + \delta_0)$ **$E_{pcm,max} = m_{water} \cdot \Delta h_{fusion}$ with $\Delta h_{fusion,water,0°C} = 332.5\ kJ/kg$

Table 2: Boundary conditions for validation measurement points for the charging and discharging

plate distance δ_0	[mm]	15		30		45	
Charging		**C2**	**C3**	**C2**	**C3**	**C2**	**C3**
$time_{measurement}$	[s] / [h]	4590 / 1.3	4630 / 1.3	7320 / 2	6320 / 1.76	15410 / 4.3	15840 / 4.4
$\dot{m}_{CO2}$	[kg/min]	7	10	7	10	7	10
p_{ref-in}	[bar]	32	32	32	32	32	32
$T_{init,pcm}$*	[°C]	10	8	15	9	10	11
Discharging		**D5**	**D6**	**D5**	**D6**	**D5**	**D6**
$time_{measurement}$	[s] / [h]	5340 / 1.5	4180 / 1.2	11370 / 3.17	9410 / 2.6	27390 / 7.6	14860 / 4.1
$\dot{m}_{CO2}$	[kg/min]	7	10	7	10	7	10
p_{ref-in}	[bar]	39	39	39	39	39	39
$\bar{T}_{init,pcm}$*	[°C]	-1.5	-0.6	-2	-0.75	-8	-5

*$\bar{T}_{init,pcm}$ = mean value T(t=0s)

Figure 6 shows the TIL testbench used for dynamic model validation of the Modelica/Dymola model.

As shown in Figure 7a, the charging case inlet refrigerant conditions are defined on the bubble line and the outlet conditions can be found time-dependent on the dew line, gas- or two-phase region. In the event of discharge, Figure 7b, shows the refrigerant inlet and outlet conditions that can be calculated using the energy balance of the secondary glycol circuit and are in the two-phase and liquid region and can therefore clearly determined including the energy balance.

For the charging case, only the refrigerant inlet conditions are known from pressure and temperature measurements at the bubble line, which enables the inlet enthalpy to be calculated. The outlet enthalpy cannot be calculated based on outlet pressure and temperature when conditions are in the two-phase region.

This is the accepted version of a paper published at GL2022
http://dx.doi.org/10.18462/iir.gl2022.0048

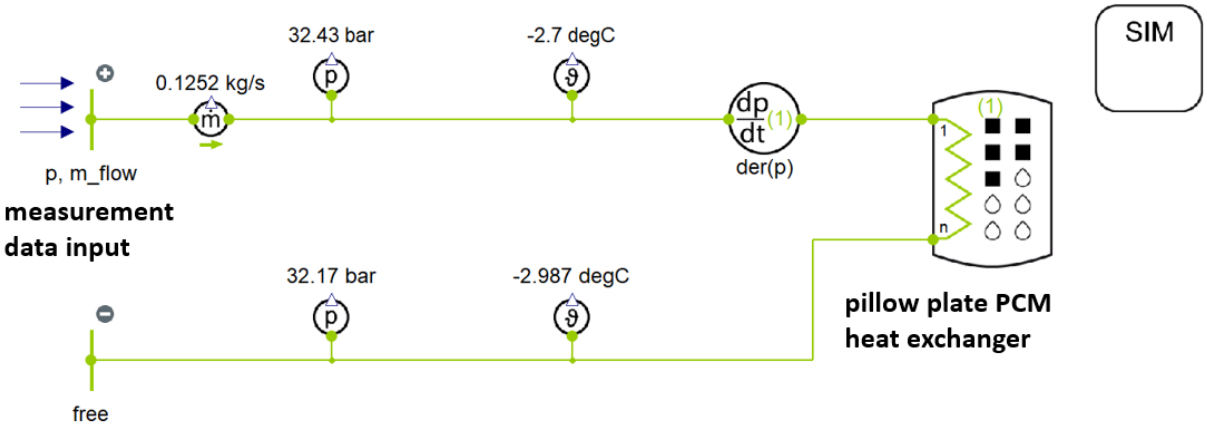

Figure 6: TIL Validation test bench.

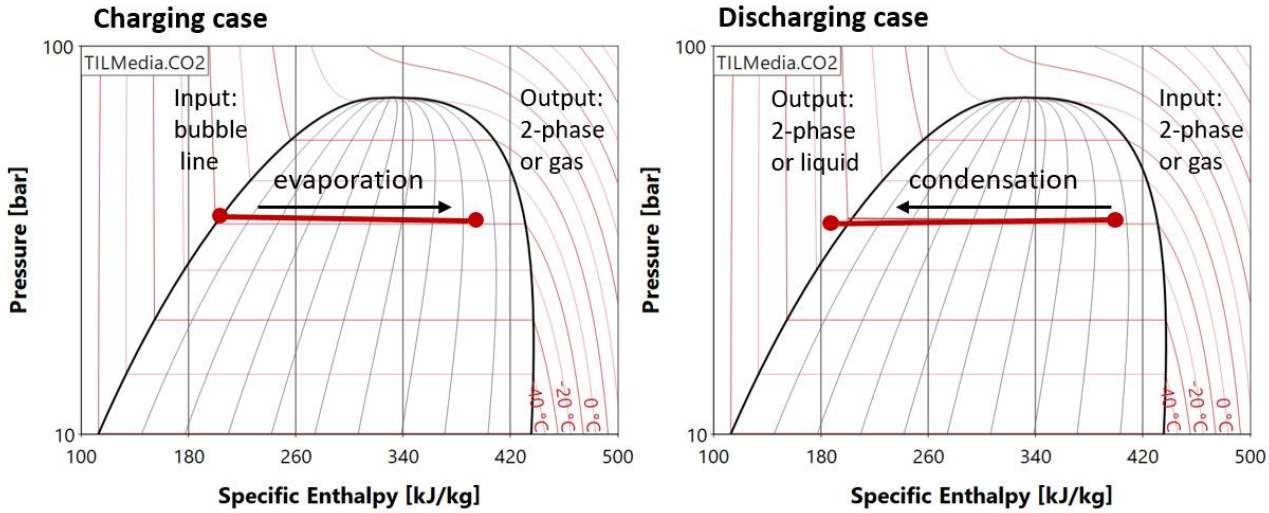

Figure 7a: CO2 side charging case and Figure 7b: discharging case plotted in the p-h-chart.

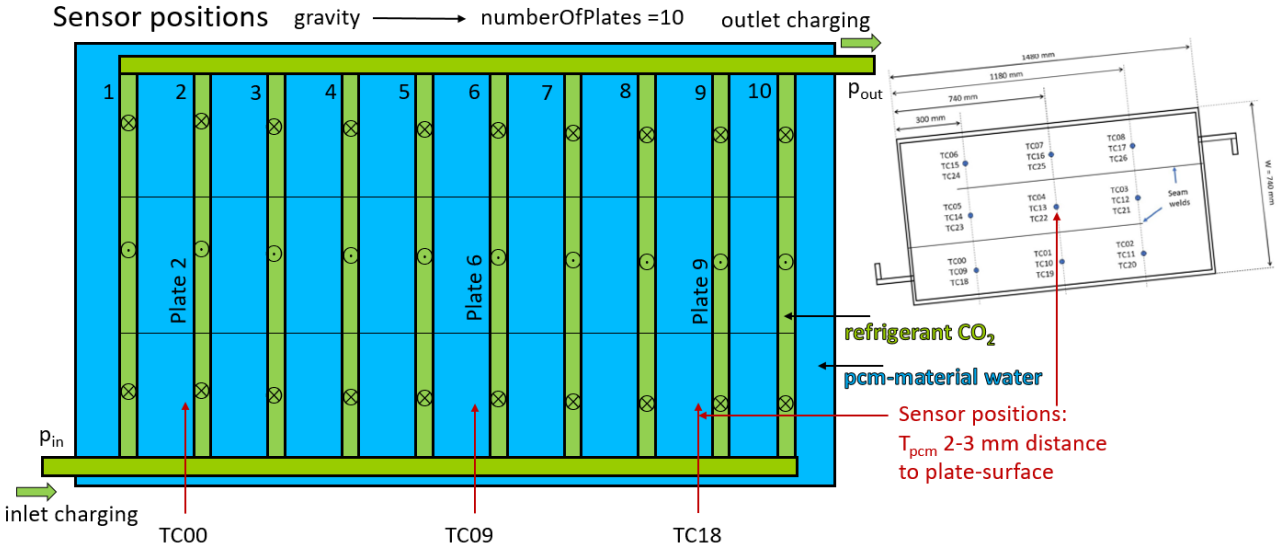

Figure 8: Temperature sensor positions of 27 sensors on Plates 2, 6 and 9 with 2-3 mm distance to plate-surface (Selvnes et al., 2021b).

This is the accepted version of a paper published at GL2022
http://dx.doi.org/10.18462/iir.gl2022.0048

4. RESULTS

Figure 9 shows simulated and measured charging temperatures for refrigerant and SLE cells plotted versus the refrigerant enthalpy for the 30-mm plate at time t = 945 s. Temperature sensors mounted in SLE material with 2-3 mm distance to plate surface in Plates 2, 6 and 9.

The model discretization is set to 9x5 (n_{VLE} x n_{SLE}): the refrigerant side is divided into 9 cells and the SLE side divided into 5 water cells perpendicular to the refrigerant flow. The length of each SLE cell is calculated from the plate spacing δ_0 and the SLE discretization n_{SLE} as follows:

$$\delta_{sle-cell-length} = \frac{\delta_0}{n_{SLE}} . \qquad \text{Eq. (17)}$$

With a plate spacing of 15, 30 and 45 mm and a discretization of 5, the sle-cell-lengths are 3, 6 and 9 mm. In all cases, the temperature sensor for the measurement is located within the first layer of the discretized cells at a distance of 2-3 mm from the plate.

The measured temperatures shown in Figure 9 mainly scatter mainly between the simulated temperatures of the first 2 cells. The refrigerant pressure drop of 0.7 bar leads to a temperature decrease of 1.4 K at an inlet pressure of 32.6 bar.

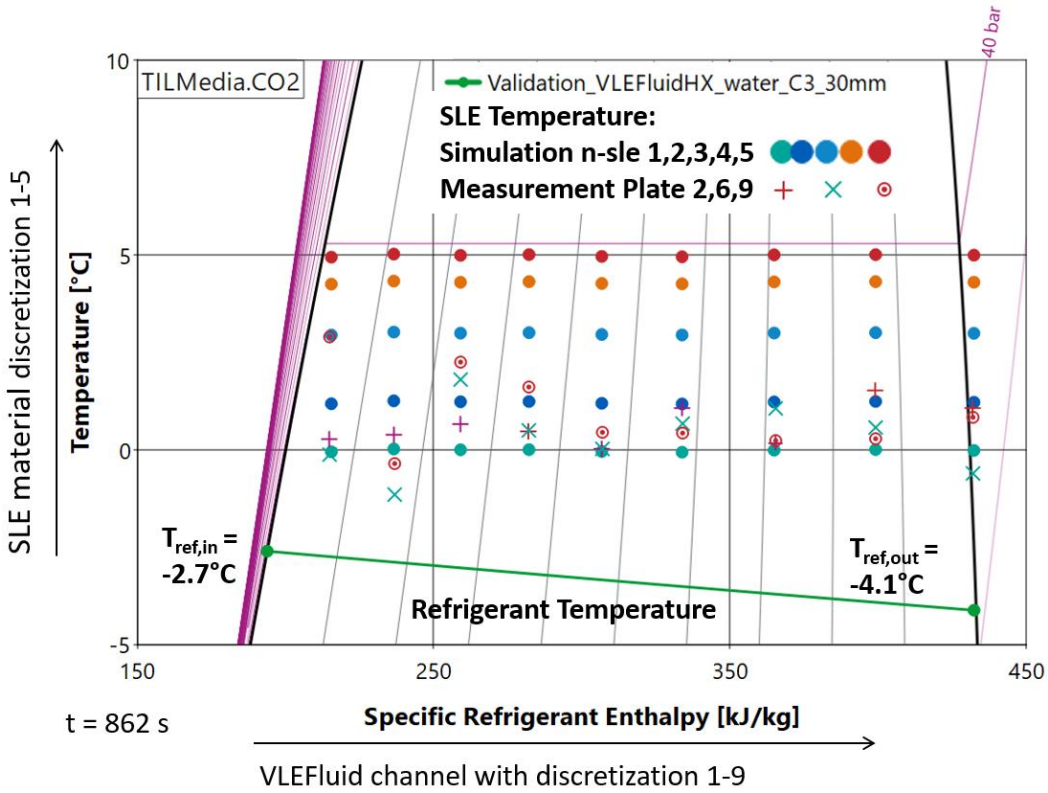

Figure 9: Simulated and measured charging temperatures for refrigerant and SLE cells plotted versus the refrigerant enthalpy for the 30-mm plate C3 at time t = 862 s. Temperature sensors mounted in SLE material with 2-3 mm distance to plate surface in Plates 2, 6 and 9.

The simulated convective heat transfer coefficients on the refrigerant side are 3000-6000 W/(m²K) for evaporation on charging 1500-3000 W/(m²K) for condensation on discharging. The values are therefore in a relatively high range that is typical for CO_2, depending on the heat transfer in the gas, two-phase or liquid range. The bottleneck is not the convective heat transfer on the refrigerant side, but the heat conduction through the PCM (water). The mean relative deviation between simulated and measured pressure drop on the refrigerant side is for the discharging approximately 3.5 %. The relative deviation of the energy balance of the simulated discharging system is in a range of 2 % within the measurement if the heat loss to the environment is neglected.

This is the accepted version of a paper published at GL2022
http://dx.doi.org/10.18462/iir.gl2022.0048

4.1. Charging Process

The measured and simulated temperature distributions for the charging process of C3-30 mm point are plotted versus time in Figure 10. The simulated charging process starts with an initial PCM temperature of 9 °C. The simulated temperatures in SLE-cells 1 and 2 are plotted for each refrigerant cell 1-9. The measured 27 water temperatures were averaged over the measuring points on Plates 2, 6 and 9 to 9 mean values plotted in Figure 9. Furthermore, the mean SLE inlet and outlet temperatures (summary.T_sle_A/B) averaged over the SLE discretization are shown. The discretization of the SLE cells causes steps features in the simulated temperature profile, while the measured data shows only small fluctuations, which are partly due to supercooling effects. The measured values are about in the area between the simulated temperature of the SLE-cells 1 and 2 and show good agreement with the simulation. The average values (summary.T_sle_A/B) at inlet and outlet show significantly higher values due to consideration of layers further away from the plate and the measurement sensors.

To determine the time required for complete charging, the charging process simulation is extended until the last SLE/water cell is frozen, as shown in Figure 11. As boundary conditions, the experimental data for C3 – 30 mm were taken and extrapolated until complete freezing. Complete freezing occurs only after 3 hours.

Figure 12 shows the simulated charge curve plotted versus time as the ***relative charge***

$$E_{pcm,charge,rel} = \frac{\int_0^t \dot{Q}_{ref}}{m_{water} \cdot \Delta h_{fusion}} . \qquad \text{Eq. (18)}$$

At the end of the experiment, the storage is 88 % charged within a period of 1.8 h. The time for full charge is 3 h and the relative charge is more than 100 % at 115 % due to the additional sensible heat of the water. The kinks in the charging curve result from the discretized SLE cell geometry and the temperature steps seen in Figure 11.

4.2. Discharging Process

Similar to the charging process, Figure 13 shows the simulated and measured dynamic temperature distribution for the discharging process plotted versus time for the D6-30 mm point. The simulated discharging process starts with an initial PCM temperature of -0.75 °C. The simulated temperatures in SLE-cells 1 and 2 are plotted for each refrigerant cell 1-9. The measured 27 water temperatures were averaged over the measuring points on Plates 2, 6 and 9 to 9 mean values plotted in Figure 13. Furthermore, the mean SLE inlet and outlet temperatures (summary.T_sle_A/B) averaged over the SLE discretization are shown. The measured values are about in the area between the simulated temperature of the SLE-cells 1 and 2 and show good agreement with the simulation.

To determine the required time for complete discharging, the discharging process simulation is extended until the last SLE/water cell is melted, as shown in Figure 14. As boundary conditions, the experimental data for D6 – 30 mm were taken and extrapolated until complete freezing. Complete melting occurs only after 14 hours.

Figure 15 shows the simulated discharge curve plotted versus time as the ***relative charge***

$$E_{pcm,discharge,rel} = 1 - \frac{\int_0^t \dot{Q}_{ref}}{m_{water} \cdot \Delta h_{fusion}} . \qquad \text{Eq. (19)}$$

At the end of the experiment, the storage is 54 % charged within a period of 2.6 h. The time period for complete zero charge is 14 h.

This is the accepted version of a paper published at GL2022
http://dx.doi.org/10.18462/iir.gl2022.0048

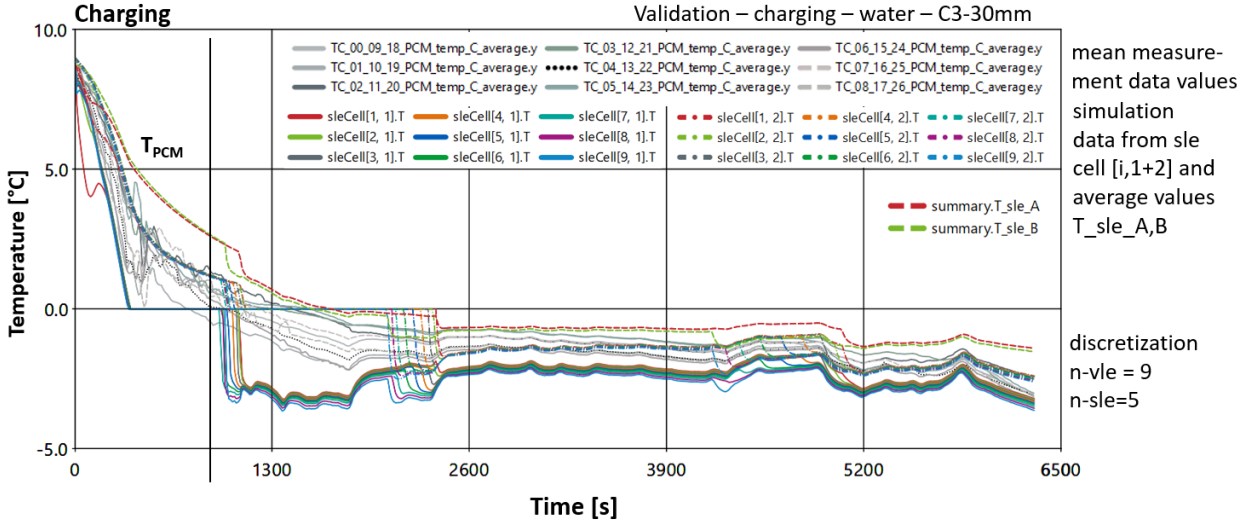

Figure 10: Simulated and measured charging temperature profile versus time for C3 - 30 mm plate.

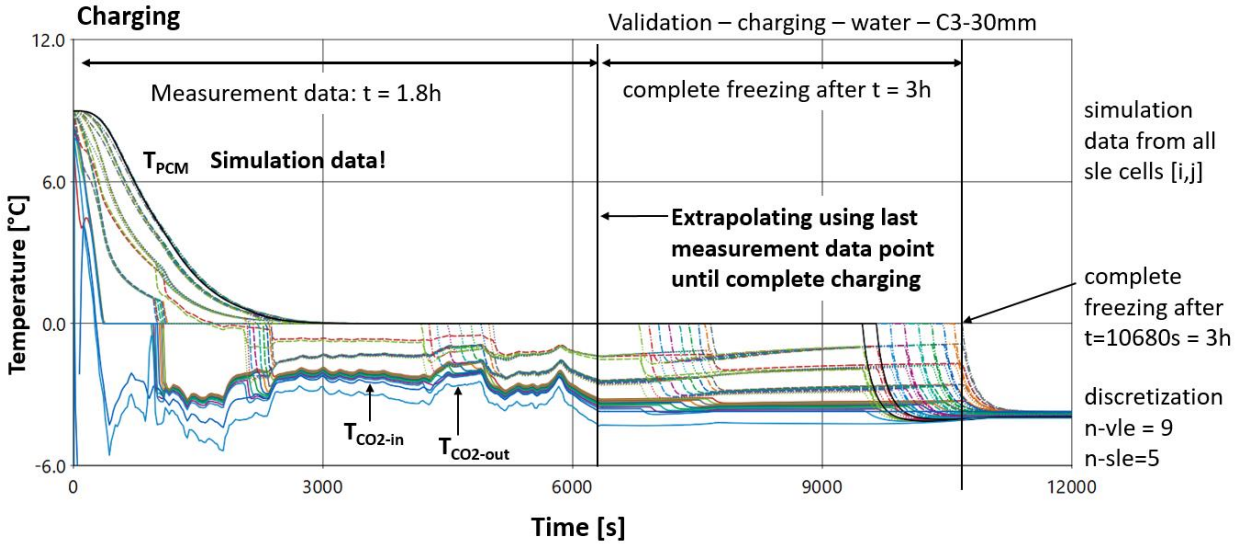

Figure 11: Simulated charging temperature profile versus time for C3 - 30 mm plate. Extrapolation until complete freezing of PCM (water).

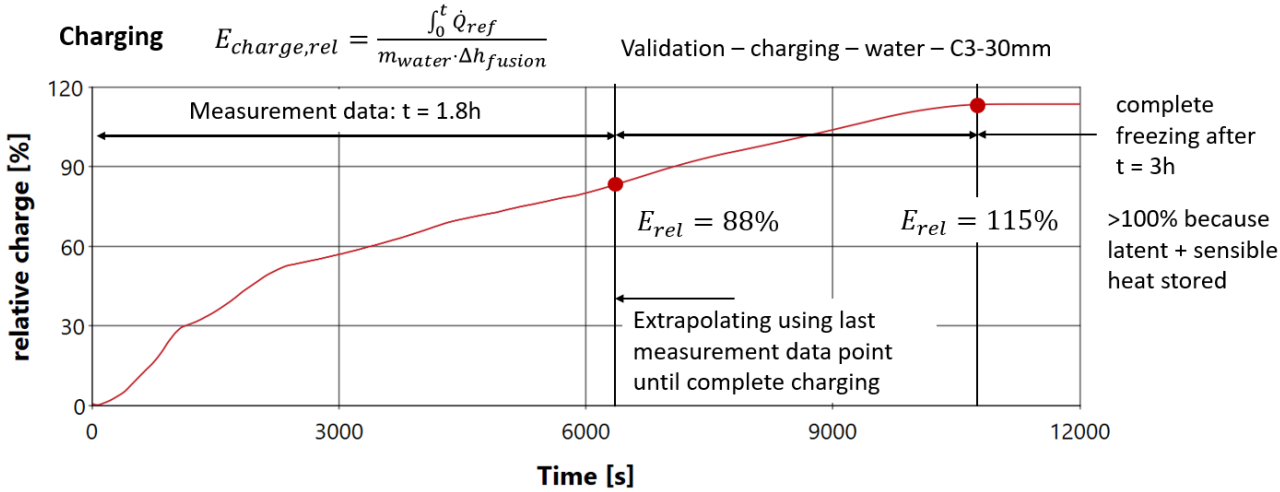

Figure 12: Simulated relative charging curve versus time for C3 - 30 mm plate.

This is the accepted version of a paper published at GL2022
http://dx.doi.org/10.18462/iir.gl2022.0048

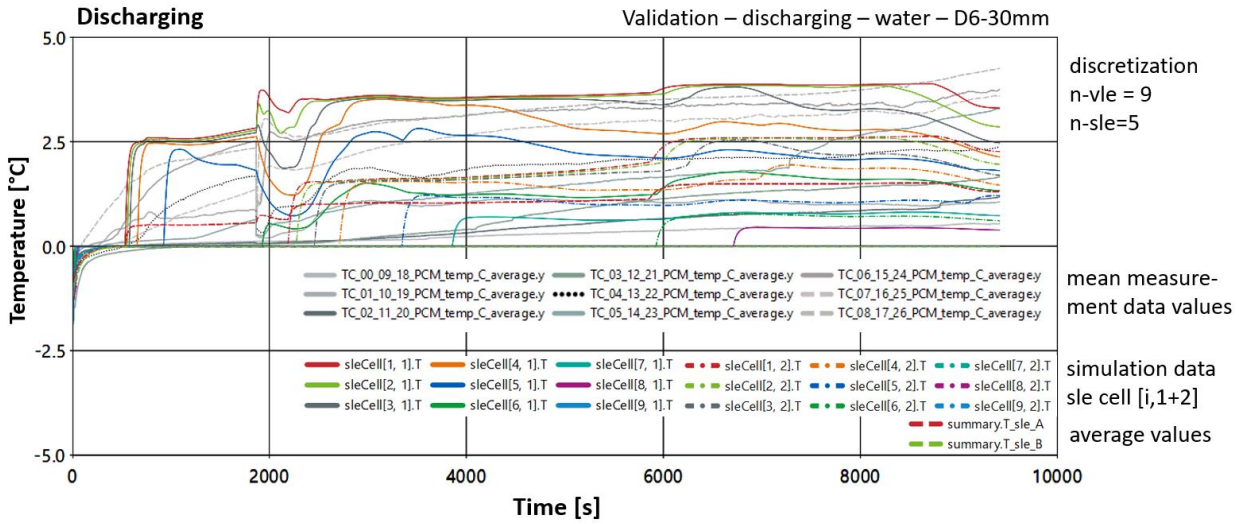

Figure 13: Simulated and measured discharging temperature profile versus time for D6 - 30 mm plate.

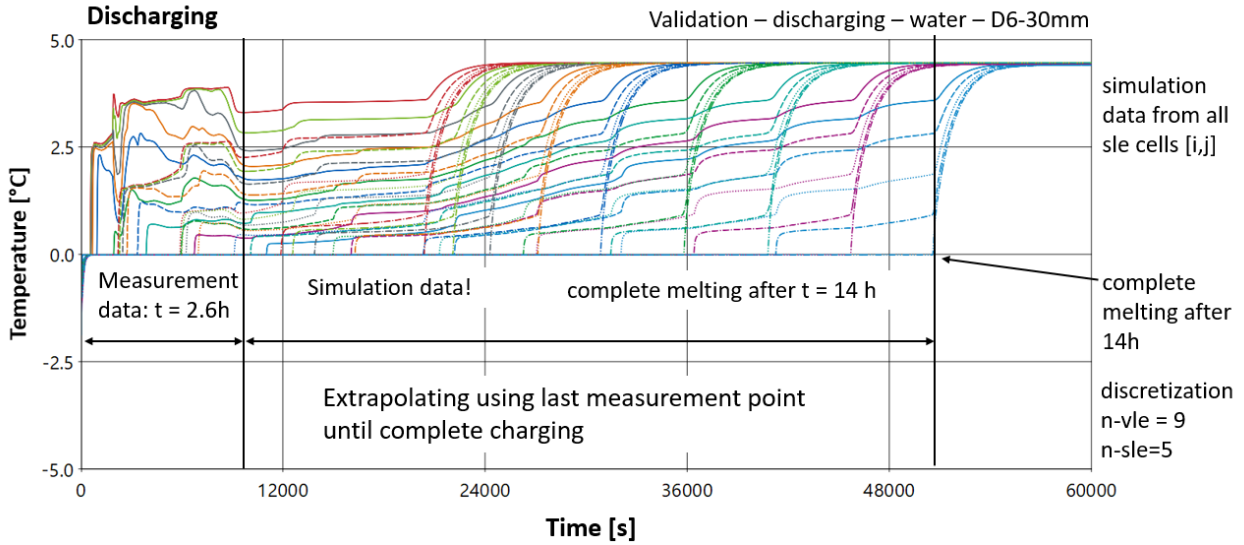

Figure 14: Simulated discharging temperature profile versus time for C6 - 30 mm plate with extrapolation until complete melting of PCM (water) material.

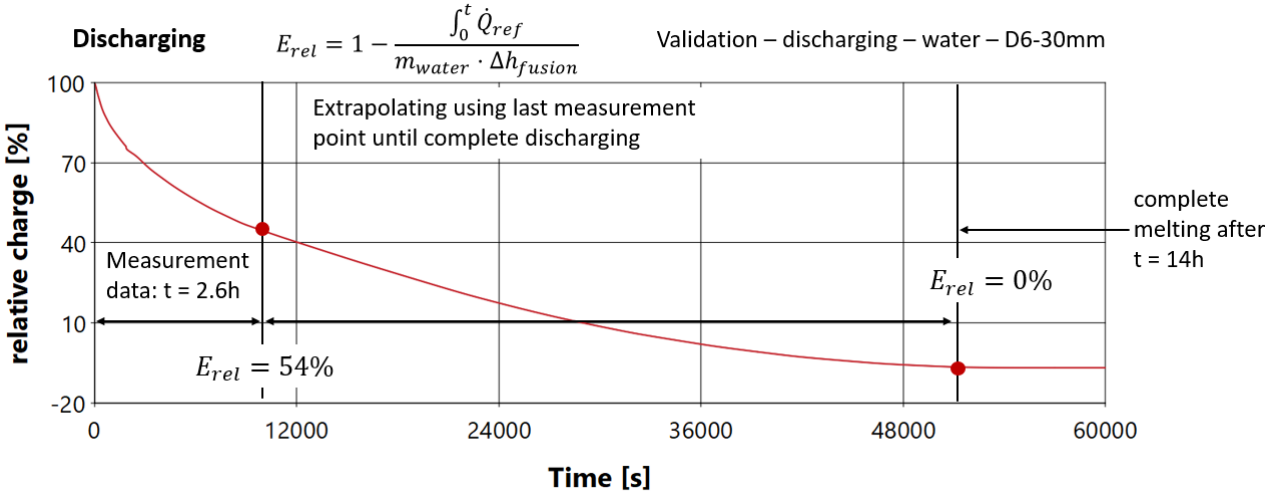

Figure 15: Simulated relative discharging curve versus time for D6 - 30 mm plate.

A summary of the simulation and measurement results for different plate geometries for charging and discharging is shown in Table 3. The period of the measurement time, simulation of 100 % charging and 100 % discharging and the energy content in kWh and rel. PCM charge for charging and discharging case.

Table 3: Simulation and measurement results for different plate geometries for charging and discharging.

Charging + discharging with water as pcm $E_{pcm,max} = m_{water} \cdot \Delta h_{fusion}$ $\dot{Q}_{ambient,loss} \cong 0$!

plate distance δ_0	[mm]	15		30		45	
Charging		**C2**	***C3***	**C2**	***C3***	**C2**	***C3***
$time_{measurement}$	[s]	4590	4630	7320	6320	15410	15840
$time_{simulation}$ 100% filled	[s]	3100	2660	12250	10680	29400	32200
$E_{charge,100\%\ filled}$ *	[kWh]	13.5 *(13.6)*⁺	13.1 *(13.1)*⁺	30.1 *(22.5)*⁺	30 *(21.3)*⁺	45 *(32.4)*⁺	45 (32.2)⁺
$E_{pcm,charge,rel.}$ **	[%]	115%	111%	120% *(88%)*	115% *(84%)*	115% *(83%)*	115% (82%)
Discharging		**D5**	***D6***	**D5**	***D6***	**D5**	***D6***
$time_{measurement}$	[s]	5340	4180	11370	9410	27390	14860
$time_{simulation}$ 100% emptied	[s]	14250	14890	46800	50660	97303	95820
$E_{charge,100\%\ emptied}$ *	kWh	11.6 *(9.8)*⁺	11 *(8)*⁺	25 *(16)*⁺	25 *(12.7)*⁺	39 *(28)*⁺	*39 (19)*⁺
$E_{pcm,discharge,rel.}$ ***	%	0% *(10%)*⁺	0% *(29%)*⁺	0% (31%)⁺	-6% *(46%)*⁺	0% *(25%)*⁺	0% *(47%)*⁺
		⁺with regard to measurement time					

* $E_{charge/discharge} = \int_0^t \dot{Q}_{ref}$ ** $E_{pcm,charge,rel} = \frac{\int_0^t \dot{Q}_{ref}}{m_{water} \cdot \Delta h_{fusion}}$ *** $E_{pcm,discharge,rel} = 1 - \frac{\int_0^t \dot{Q}_{ref}}{m_{water} \cdot \Delta h_{fusion}}$

5. CONCLUSIONS

The current study presents a numerical model of a CTES unit using water as PCM the storage medium and CO_2 as refrigerant. The model was developed for both component design and system simulation and can be used to optimize and study the heat exchangers and systems. The heat exchanger in the CTES unit consists of a stack of stainless-steel pillow plates immersed into a stainless-steel container filled with water as PCM melting and freezing at 0 °C. The charging and discharging processes of the PCM-CTES unit are carried out through evaporation and condensation of the CO_2 circulating inside the plates, respectively. The dynamic model of the PCM-CTES unit is developed in the object-oriented programming language Modelica using the component library TIL-Suite. The model of the PCM-CTES unit is validated by using previously published experimental data from a test facility with an identical setup. Various heat exchanger configurations, storage medium and refrigerant parameters are tested, and the model demonstrates good agreement with the experimental data for both dynamic charging and discharging cases using different geometries with different plate distances. The model allows flexible use with different PCMs in different temperature ranges and thus enables a wide range of possible uses in future applications.

ACKNOWLEDGEMENTS

This study was carried out through the research project KSP PCM-STORE (308847) supported by the Research Council of Norway and industry partners. PCM-STORE aims at building knowledge on novel PCM technologies for low-temperature thermal energy storage.

NOMENCLATURE

CTES	Cold Thermal Energy Storage	*A*	area [m²]
HT	heat transfer	*b*	thickness [m]
hyd	hydraulic	*c*	specific heat capacity [J/(kg K)]
ini	initialization	*E*	Energy [J]

This is the accepted version of a paper published at GL2022
http://dx.doi.org/10.18462/iir.gl2022.0048

max	maximum	*d*	Diameter [m]
min	minimum	*h*	specific enthalpy [J/kg]
PCM	Phase Change Material	*i*	index
SLE	Solid Liquid Equilibrium	*j*	index
TES	Thermal Energy Storage	*m*	mass [kg]
VLE	Vapor Liquid Equilibrium	*n*	index
		p	pressure [bar]
δ	thickness [m]	*q*	quality [-]
Δ	delta [-]	*T*	Temperature [°C]
λ	thermal conductivity [W/(m K)]	*V*	Volume [m³]
ρ	density [kg/m²]	*w*	wall

REFERENCES

Baehr, H.D., Stephan, K., 1996. Wärme- und Stoffübertragung. Springer 2nd Edition.

Bony, J., Citherlet, S., 2007.Comparison between a new TRNSYS model and experimental data of phase changer materials in a solar combisystem. Proceedings Building Simulation, 371-378.

Collier, J.G., Thome, J.R., 1996. Convective Boiling and Condensation. 3rd Edition, 1996

Fidorra, N., Hafner, A., Minetto, S., Köhler, J., 2015. LOW TEMPERATURE HEATSTORAGES IN CO2 SUPERMARKET REFRIGERATION SYSTEMS. 24thIIR International Congress of Refrigeration, Yokohama, Japan.

Fidorra, N., Minetto, S., Hafner, A., Banasiak, K., Köhler, J., 2016. Analysis of Cold Thermal Energy Storage Concepts in CO2 Refrigeration Systems. 12th IIR Gustav Lorentzen Natural Working Fluids Conference, Edingburgh, UK.

Fidorra, N., Kistner, J., Tegethoff, W., 2021. Energieflexibilisierung im Supermarkt. Presentation DKV-Jahrestagung, Dresden, Germany.

Hafner, A., Nekså, P., 2018. Integrated CO_2 solutions for supermarkets. 13th Gustav Lorentzen Conference, Valencia, Spain.

Jokiel, A., Sevault, A., Banasiak, K., Næss, E., 2021. Cold storage using phase change material in refrigerated display cabinets: experimental investigation. 13th IIR Conference PCM 2021, Italy, September 1-3.

Manescu, R., Hafner, A., Fidorra, N., Försterling, S. Köhler, J., 2017. A new approach for cold thermal energy storages in supermarket refrigeration systems. 7th IIR Conference, Ammonia and CO2 Refrigeration Technologies, Ohrid, Macedonia.

Mehling, H. and Cabeza, L. F., 2008. Heat and cold storage with PCM. An up to date introduction into basics and applications. Springer Verlag, ISBN: 978-3-540-68556-2, Berlin, Germany.

Mitrovic, J. and Maletic, B., 2011. Numerical Simulation of Fluid Flow and Heat Transfer in Thermoplates. Chem. Eng. Technol, 34, No. 9, 1439-1448.

Modelica Association, 2022. Modelica and Modelica Standard Library. https://modelica.org/ (access January 6, 2022).

Neumann, Hannah, 2020. Untersuchung eines Latentwärmespeichers für Prozessanwendungen. PhD-Thesis, University of Freiburg in Breisgau, Germany.

Piper, M., Olenberg, A., Tran, J.M., Goedecke, R., Scholl, S., Kenig, E.Y., 2014. Bestimmung charakteristischer Geometrieparameter von Thermoblech-Wärmeübertragern. Chemie Ingenieur Technik, 86, No. 8, 1214-1222

This is the accepted version of a paper published at GL2022
http://dx.doi.org/10.18462/iir.gl2022.0048

Piper, M., Olenberg, A., Tran, J.M., Kenig, E.Y., 2015a. CFD-Untersuchung der Fluiddynamik und des Wärmeübergangs bei einphasiger Strömung im welligen Spalt zwischen Thermoblechen. Chem. Ing. Tech., 87, No. 3, 216-225.

Piper, M., Tran, J.M., Kenig, E.Y., 2015b. Determination of the geometric design parameters of pillow-plate heat exchangers. Applied Thermal Engineering, 91, 1168-1175.

Richter, Christoph, 2008. Proposal of New Object-Oriented Equation-Based Model Libraries for Thermodynamic Systems. PhD thesis, TU Braunschweig, Germany.

Schulze, C., 2013, A Contribution to Numerically Efficient Modelling of Thermodynamic Systems. PhD thesis, TU Braunschweig, Germany.

Selvnes, H., Hafner, A., Kauko, H., 2019. Design of a cold thermal energy storage unit for industrial applications using CO_2 as refrigerant. 25th IIR International Congress of Refrigeration. ID: 139.

Selvnes, H., Allouche, Y., Sevault, A., Hafner, A., 2019a. CFD modelling of ice formation and melting in horizontally cooled and heated plates. Eurotherm Seminar #112 Advances in Thermal Energy Storage, University de Lleida, Spain.

Selvnes, H., Allouche, Y., Sevault, A., Hafner, A., 2019b. A CFD analysis for the performance assessment of a novel design of plates-in-tank latent storage unit for freezing applications. 8th Conference on Ammonia and CO2 Refrigeration Technologies, Ohrid, Macedonian, DOI: 10.18462/iir.nh3-co2.2019.0041.

Selvnes, H., Allouche, Y., Manescu, R. Hafner, A. 2021a. Review on cold thermal energy storage applied to refrigeration sytems using phase change materials. Thermal Science and Engineering Progress 22, 100807.

Selvnes, H., Allouche, Y., Hafner, A. 2021b. Experimental characterisation of a cold thermal energy storage unit with a pillow-plate heat exchanger design. Applied Thermal Engineering. vol. 199.

Sevault, A., Banasiak, K., Bakken, J., Hafner, A., 2018. A novel PCM accumulator for refrigerated display cabinet: design and CFD simulations. 12th IIR Conference PCM 18, Orford (Québec), Canada, May 21-23.

Sevault, A., 2020. PCM-Store – Solving thermal energy storage challenges in support of a more energy-efficient food industry. Sintef KPN-project funded by partners and the Research Council of Norway, https://www.sintef.no/projectweb/pcm-store/ (January 10, 2022)

Shah, M.M., 1979. A general correlation for Heat Transfer during film condensation inside pipes. Int. J. Heat Mass Transfer, Vol. 22, 547-556

Swamee, P.K., Jain, A.K., 1976. Explicit Equations for Pipe-Flow Problems. Journal of the Hydraulics Division, 102, 657-664

Tegethoff, W. et al., 2011. TEMO-Thermisch Echtzeitfähige Modelle, Braunschweig,Germany, 2011

Tran, J.M., Piper, M., Kenig, E. Y., Scholl, S., 2018. Pillow-Plate Heat Exchangers: Fundamental Characteristics. In: Bart, H.M and Scholl, S., Innovative Heat Exchanges. Springer book ISBN 978-3-319-71639-8, 233.

VDI-Wärmeatlas, 2013. 11th edition, Editor VDI e.V., Düsseldorf, Germany.

This is the accepted version of a paper published at GL2022
http://dx.doi.org/10.18462/iir.gl2022.0048